CR-171 928

IN VIVO NUCLEAR MAGNETIC RESONANCE IMAGING

CONTRACT NAS9-16442, P3

FINAL REPORT - OCTOBER 1984

DEPARTMENT OF MEDICINE
BAYLOR COLLEGE OF MEDICINE

(NASA-CR-171928) IN VIVO NUCLEAR MAGNETIC RESONANCE IMAGING Final Report, Oct. 1984 (Baylor Coll. of Medicine) 25 p
HC A02/MF A01 CSCL 06P G3/52

N86-21105
Unclas
08475

Principal Investigator: Adrian LeBlanc, Ph.D.

Co-Investigators: Harlan Evans, Ph.D.
R. Nick Bryan, M.D.
Phillip Johnson, M.D.
Ernie Schonfeld, M.S.
Satish G. Jhingran, M.D.

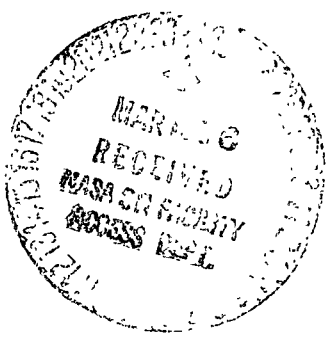

SUMMARY

A number of physiological changes have been demonstrated in bone, muscle and blood after exposure of humans and animals to microgravity. Determining mechanisms and the development of effective countermeasures for long duration space missions is an important NASA goal. Historically, NASA has had to rely on measuring tapes, x-ray and metabolic balance studies requiring collection of excreta and blood specimens to study this problem. The advent of tomographic nuclear magnetic resonance imaging (NMR or MRI) gives NASA a way to greatly extend early studies of this phenomena in ways not previously possible; NMR is also noninvasive and safe. NMR provides both superb anatomical images for volume assessments of individual organs and quantification of chemical/physical changes induced in the examined tissues. The purpose of this work is to determine and demonstrate the feasibility of NMR as a tool for human physiological research as it is affected by microgravity.

The animal studies employed the rear-limb suspended rat as a model of muscle atrophy that results from microgravity. This technique unloads the rear limbs without immobilization and causes a caudal shift in body fluid similar to spaceflight. NMR measurements were made using a number of resonant frequencies (100, 20, 10 MHz) and after various periods of limb suspension. Despite significant muscle atrophy (soleus and gastrocnemius) and blood flow changes, none of the NMR measurements (T_1, T_2, T_2 diffusion) demonstrated a significant change. This data suggests that atrophy itself will present a different NMR spectrum than pathological induced atrophy. Also, volume measurements of atrophied muscle will not be affected by concomittant changes due to muscle atrophy.

Bedrest of normal male subjects was used to simulate the effects of microgravity on bone and muscle. A technique was developed to image the lower limbs of subjects before and after bedrest which includes an improved method for producing images calculated from T_2, a computer scheme for classifying tissue according to different T_2 relaxation times and quantifying tissue volumes. To date, six bedrest subjects have been imaged before and after bedrest. Based on cross-sectional images through the lower leg, the gastrocnemius and soleus muscle areas decreased 9% while total muscle area in this same section decreased 6%, demonstrating differential muscle loss. Bone marrow T_2 was decreased 14% ($P < 0.001$) after bedrest indicating an increase in marrow fat, a change which may be related to red cell mass and bone changes observed after exposure to weightlessness or bedrest. Muscle T_2 did not change, suggesting that tissue hydration is not changed by atrophy.

With the acquisition of the 2.3 Tesla system by Baylor in early 1985, these studies will be extended to high energy phosphate measurements. A technique to display fat and H_2O proton quantitative images simultaneously will be investigated and techniques to measure vessel and/or limb muscle blood flow will be developed. Limb investigations will be extended to muscles in the back and bone marrow in the spinal vertebrae.

BACKGROUND

a. Development of Nuclear Magnetic Resonance Imaging

In 1946, Bloch, Hanson, Purcell and Pound showed that certain elements give rise to observable nuclear magnetic resonances (1-4). Magnetic moments, oriented in a random fashion in the absence of a magnetic field, align themselves within an external field in a limited number of orientations. The energy resulting from changes between states lie within conventional radio frequency (rf) bands. Hence, magnetically aligned or polarized nuclei may be detected by energizing them with incident rf waves. The resultant NMR signals characterize many aspects of the chemical and physical state of a sample. Significantly, NMR is a noninvasive technique in the sense that the chemical nature of the investigated material is not altered.

High-resolution NMR spectrometry has been applied in biochemistry with increasing regularity. Its ability to investigate biologically important molecules using probes for hydrogen, phosphorus, carbon and nitrogen has resulted in substantial progress in the analysis of complex biological compounds. Recently, high-resolution NMR methods have been adapted to in vivo studies of ^{31}P. These experiments rest on the ability to distinguish in the intact animal several phosphorus compounds - inorganic (iP), carbohydrate phosphorus, phosphocreatinine (PCr), ATP, and perhaps ADP . For these experiments, excitation and detection are done by an rf coil attached to the sample, surface coils. In general, it detects material close to the coil and it has been used to study ^{31}P of skeletal and heart muscles, kidney, liver and brain (5). Ackerman et al have shown PCr to ATP ratios of 1.93 which is higher than the best values attained by in vitro rapid freezing techniques, suggesting a nearly instantaneous start to the degradation process. In addition, they found that mobile ADP and iP concentrations determined by NMR were much lower than in other analytical techniques. They and others have reported that localized ischemia of rat muscle and brain produce significant differences in the ^{31}P spectra. Ischemic tissue has lower PCr and ATP values and a markedly higher iP. They observed also a chemical shift in iP indicating a lower tissue pH (6-10). NMR techniques offer great potential in the investigation of acute ischemic tissue metabolism.

Typical high-resolution proton NMR experiments assume that NMR signals indicate the total number of nuclei observed, or the spin density (SD) of the sample. While this may be true under precisely defined conditions, the observed SD, in complex compounds and tissues is altered by two other NMR parameters, the transverse, or spin-spin (T_2) and longitudinal, or spin-lattice (T_1), relaxation times. Differences in T_2 and T_1 reveal molecular level organizational differences. It is convenient to think of relaxation times as memories. The phase memory, or T_2, is "short-term", i.e., 10-200 msec while the polarization memory, or T_1 is "long-term", i.e., 150-1500 msec in biological tissues (11-12). Measurement of relaxation times has been used to evaluate water in the complex forms it exists in biological tissues. This technique can characterize some of the physical properties of hydrogen nuclei (mainly H_2O) in biological samples and allow differentiation of normal organ tissue from pathologic tissues. While it is an empirical fact that different tissues have distinctive proton NMR

parameters, a proven theoretical basis for these variations in biologic samples is not available (13-16).

In the 1960's and early 1970's several investigators, including Damadian and Lauterbur in the United States and Mansfield and Hinshaw in England, modified high resolution NMR for the partial chemical analysis of relatively small volumes with coincident identification of the spatial coordinates of the analyzed volume (17-23). If these data are obtained from a tissue sample, images based on tissue chemistry can be formed. This important step has led to a recent flurry of interest in NMR in vivo imaging called zeugmatography or NMR tomography. NMR imaging is now undergoing initial clinical trials and has been shown to have excellent anatomic resolution. Early results also indicate that the technique provides unique pathologic information (24-27).

b. Physiological Changes from Exposure to Microgravity and from Disuse

In this section we do not attempt to exhaustively review the literature but will summarize major animal or human findings from spaceflight, bedrest, and animal modeling of spaceflight as they relate to the proposal, i.e., application of NMR techniques.

Limb volume change associated with exposure to microgravity probably involves two factors: 1) Loss of fluid and changes in venous pooling followed subsequently by; 2) Muscle atrophy. Both processes involve fluid shifts, one mostly extracellular, the second intracellular. NMR techniques are ideal for measuring changes in water content of tissues and is both noninvasive and quantitative.

Urinary nitrogen excretion has been shown to be increased in bedrest and during weightlessness indicating muscle wasting or deconditioning (28-31). Muscle wasting would be expected to produce muscles less able to perform work. Muscular deconditioning was documented during Apollo and Skylab missions and has been shown in bedrest subjects (32). Pre and post flight muscle strength testing in Skylab demonstrated that an adequate exercise program may have been devised which protected the arm muscles against wasting. Locomotion in weightlessness uses the arms more than the legs. Not surprisingly, exercise regimes designed to protect the leg muscles were only partially successful. Leg volume changes in Skylab 2 and 3 were about -4.5% while in Skylab 4 they were approximately -2%. Presumably, the smaller loss of leg volume by the Skylab 4 crew was due to an increase in programmed and personal preference daily exercise which occurred. This is supported by the leg strength measurements which showed a similar pattern, i.e., -25% loss after Skylab 2 vs. -8% loss after Skylab 4. These results suggest that a properly designed exercise program might preserve muscle volume and strength even during long duration missions.

The muscle volume loss and the strength loss produced by weightless exposure probably affects some muscles more than it does others. In Skylab data this was suggested by the observed differences between the leg flexors and extensors. Prior to NMR there would be no way in which this could be studied in the intact human except by the Skylab methods of estimating differential strength which are subject to error because of psychological factors. It is also not possible to differentiate soleus from gastrocnemius

which are both extensors. Estimating back muscle strength may be even more difficult.

Animal studies have shown that differential muscle atrophy (soleus vs. gastrocnemius) occurs with weightlessness and in animal models of weightlessness but not with immobilization. Cast immobilization of the rear limbs of rats for 21 days produces a 52% and 45% atrophy by weight of the soleus and gastrocnemius muscles, respectively (40,41). Similarly, immobilization of the knee and ankle joints produces a 58% loss of the soleus mass within two weeks (42). Tenotomy produces a 25% decrease in the gastrocnemius in three weeks, and a decrease of 50% by 4 - 9 weeks (43). Nerve resection causes a 50% weight loss in the gastrocnemius by 4 - 5 weeks (44). Young rats suspended for two to three weeks showed a 40 - 45 % and a 15 - 20 % loss in the soleus and gastrocnemius, respectively (45). Rear limb suspension of older rats for up to 90 days showed similar muscle loss which maximized by the 30th day (46). Rats flown aboard the Cosmos spacecraft for approximately 2 weeks demonstrated similar differential muscle loss in the soleus and gastrocnemius (47).

We have shown that leg area measurements using NMR are possible with a precision of about 0.2%; fat and muscle cross-sectional area may be accurately measured in a given anatomical section; differential muscle atrophy can be investigated (soleus vs. gastrocnemius) along with tissue hydration changes. It may also be possible to distinguish intracellular from extracellular water (33).

Limb immobilization reportedly alters the percentage of slow twitch muscle fibers in the soleus to the extent that twitch characteristics become similar to that of a fast twitch muscle (41). This is supported by our measurements of relative blood flow in suspended rats, i.e., the ratio of soleus to gastrocnemius blood flow of 2.3 in controls is reduced to 1.4 in suspended animals (46). Reis (48) concluded that there is a high correlation between blood flow and contraction time in normal skeletal muscle. It is reasonable then that the blood flow of the two muscles would become similar as the fiber twitch characteristics become similar. The ATP and Phosphocreatinine (Pcr) concentration of fast twitch muscle is about double that of slow twitch while the inorganic phosphate (iP) concentration in fast twitch is half that of slow twitch (49). Using NMR surface coils placed over these respective muscles the P-31 spectra of ATP, Pcr, iP can be used to monitor these high energy phosphate changes (50-52) and therefore noninvasively monitor changes in fiber type.

In Skylab a crude estimate of limb blood flow, through the belly of the gastrocnemius, was obtained by using an occlusion cuff and a leg volume measuring band (55). Measurements taken during flight suggest that limb flow was elevated compared to pre and post flight measurements. This is interesting because in contrast we find that muscle blood flow in suspended rats, an analogue of weightlessness, was probably decreased (46). NMR can be used for monitoring changes in blood flow (34-39).

Fluid shifts were documented in Skylab by visual observations of blood vessel distention, rapid changes in limb volume, center of mass measurements and subjective description such as puffy faces and head fullness (56). The spin density NMR image is essentially equal to hydrogen density which

is closely related to water content. A total or partial body spin density survey of bedrest subjects could give quantitative data regarding fluid shift not possible by any other technique.

It has been reported that the muscle water content of biopsied soleus muscles decreased following 8 hours of head down tilt bedrest (53). Tissue, T_1 and T_2 values are very sensitive to tissue water. For example a 2% change in tissue water may produce a 16% change in the relaxation time of tissue (54).

It is generally accepted that osteoporosis as well as disuse bone atrophy from bedrest and presumably spaceflight results from a relative increase of bone resorption over formation (57-62). Ultimately this manifests itself as a lower bone mineral content characterized by a larger medullary canal width and a smaller cortical width and area. For longitudinal studies a morphometric measurement of bone along with densitometry would be most useful. Because of the inherently large contrast between the bones and soft tissue NMR signals, NMR imaging is a noninvasive way for performing longitudinal bone morphometry studies.

It is known from bone biopsies that marrow fat increases 100% during the first 20 weeks of paralysis (63). Rats flown aboard Cosmos (19-21 days) have shown increases in marrow fat of 150 - 200 % in the tibia and humerus while rats undergoing rear limb suspension have shown even larger increases, +685 and +500% in marrow fat of the tibia and humerus respectively as well as decreases in bone formation (64).

The exact function of marrow adipose cells and their relation to bone metabolism and hemopoiesis is unknown. The hematological changes and the theoretical basis for these changes resulting from weightlessness are documented elsewhere and will not be discussed (65). It is known that bone marrow adipose cells have a reciprocal relationship to hemopoietic tissue. As the hemopoietic tissue expands the lipid fraction of the adipose cells decreases while the opposite occurs during decreases in hemopoiesis. Thus the metabolic activity of the marrow adipose cells are coupled to the hemopoietic activity of the marrow. In response to acute and total starvation lipolysis occurs in the extramedullary cells but not in the marrow adipose cell which continue to produce fat at an unaltered rate (66). In contrast to its remarkable resistance to starvation, the marrow adipose cell is highly sensitive to hemopoietic stimuli. The primary function therefore of marrow adipose cells appears to be related to the intensity of hemopoiesis. Therefore the study of marrow fat as it relates to hematological changes in weightlessness or bedrest could provide new information concerning the loss of red cell mass during space flight. With NMR the possibility exists to monitor these changes in vivo. This is especially important since fat containing cells of long term marrow cultures are not considered equivalent to the in vivo marrow adipose cells. These studies may also have relevance to bone atrophy that occurs under these same conditions, i.e., increased fat with decreased hemopoiesis. As it is speculated that adipose cells may serve as a store of energy required for hemopoiesis, it may serve a similar purpose for control of osteocytic or osteoblastic activity.

ANIMAL EXPERIMENTS

During the first year the rat muscle measurements were completed. The enclosed tables summarize this work which includes NMR parameter measurements (T_1, T_2, T_2 diffusion) using resonant frequencies of 200 MHz, 20 MHz, and 10 MHz. Female Sprague-Dawley rats (250-300g) were suspended by the tail for periods of 90 days. Suspended animals were compared with age matched controls which were kept in individual rat cages. In both groups, water was ad libitum while the amount of food fed to the experimental group was increased slightly to maintain body weight similar to controls.

Just prior to sacrifice approximately 800K carbonized microspheres were injected into the left ventricle (LV) of the anesthetized rats via a percutaneous puncture of the LV. After sacrificing, the left soleus and the gastrocnemius were removed for NMR analysis while the right leg muscles were removed for determination of wet weight, dry weight, percent H_2O, and percent uptake of labeled microspheres. The percent uptake of labeled microspheres was normalized by muscle weight and are labeled in the tables as BF%/gm. The latter is an indicator of relative blood flow when compared with the microsphere values of the control animals (non-suspended).

The soleus atrophies about 55% in 20 days which does not increase with an additional 60 days of suspension. Similarly the gastrocnemius shows about a 25% loss in muscle mass. These changes are similar to those seen in rats flown in space but are less than that seen with other forms of immobilization. Muscle water is decreased in the soleus at 90 days while no change was seen in the gastrocnemius. Blood flow, which is 223% higher in the soleus compared to the gastrocnemius in control animals is decreased after suspension in both muscles but to a greater degree in the soleus; the soleus is only 120% higher than the gastrocnemius after suspension. This change in blood flow can be compared to the reported change in the composition of the soleus muscle with immobilization. It has been reported that the soleus, which is normally slow twitch changes to fast twitch, the predominant fiber type in the gastrocnemius.

In none of the NMR measurements performed to date was there a significant change in the NMR parameters measured. In view of the rather significant physiological changes occurring in the suspended rat muscle, this is surprising. Further work is needed before speculating as to why the NMR parameters are not altered. It does suggest that atrophy itself will present a different NMR spectrum than pathological changes in muscle. Volume measurements of atrophied muscle will not be affected by concomitant changes due to muscle atrophy.

200 MHZ MEASUREMENTS

	T_1	T_2	T_2 diff.	Net Weight (g)	$\%H_2O$	BF%/gm
			CONTROLS			
Soleus	1.336	25.2	33.5			
	1.338	30.2	37.2			
	1.553		31.1	0.1199	74.0	
	1.517	25.6	36.5			
	1.461	27.3	37.5			
$\bar{x}$	1.441	27.9	35.2	0.1433 (9)	74.0 (9)	0.371 (9)
SD	0.100	2.7	2.8	0.015	0.75	0.165
			30 DAY SUSPENDED RATS			
Soleus	1.420	28.2	35.5	0.0567	71.41	0.106
$\bar{x}$ (n)	1.420	28.2	35.5	0.0641 (9)	71.84 (9)	0.083 (6)
± SD				0.0130	1.32	0.036
			90 DAY SUSPENDED RATS			
Soleus	1.380			0.0578	65.06	
	1.429	31.3	32.7	0.0753	67.71	0.133
	1.515	28.0	35.5	0.0548	63.75	0.128
$\bar{x}$	1.441	29.6	32.6	0.0626	65.51	0.130
± SD	0.068	2.3	0.1	±0.011	2.02	0.004

200 MHZ MEASUREMENTS

	T_1	T_2	T_2 diff.	Net Weight (g)	$\%H_2O$	BF%/gm
			CONTROLS			
Gastroc.	1.293	31.9	39.5			
	1.312		34.0			
	1.450	30.5	39.2	1.7405	73.22	
	1.496	31.5				
	1.702	28.8	36.4			
$\bar{x}$	1.451	30.7	37.3	2.0415 (9)	74.07 (9)	0.166 (9)
SD	0.165	1.4	2.6	0.246	2.10	0.039
			30 DAY SUSPENDED RATS			
Gastroc.	1.514	26.9	34.0	1.3678	72.47	0.085
	1.320	31.3	33.7			
$\bar{x}$	1.417	29.1	33.8	1.4923 (9)	73.18 (9)	0.069 (6)
SD	0.137	3.1	0.2	0.144	0.60	0.015
			90 DAY SUSPENDED RATS			
Gastroc.	1.619	32.2		1.3756	74.06	
	1.518	34.8	37.9	1.7386	75.77	0.099
				1.5342	73.60	0.081
$\bar{x}$	1.568	33.5	37.9	1.5495	74.48	0.090
± SD	0.071	1.8		0.182	1.14	0.013

200 MHZ MEASUREMENTS

	T_1	T_2	T_2 diff.	Net Weight (g)	$\%H_2O$	BF%/gm
			CONTROLS			
Soleus						
$\bar{x}$	1.441	27.9	35.2	0.1433 (9)	74.0 (9)	0.371 (9)
SD	0.100	2.7	2.8	0.015	0.75	0.165
Gastroc.						
$\bar{x}$	1.451	30.7	37.3	2.0415 (9)	74.07 (9)	0.166 (9)
SD	0.165	1.4	2.6	0.246	2.10	0.039
			SUSPENDED/CONTROL			
			90 DAY SUSPENSION			
Soleus	1.00	1.06	0.93	0.44	0.88	0.35
Gastroc.	1.08	1.09	1.02	0.76	1.00	0.54
			30 DAY SUSPENSION			
Soleus	0.99	1.01	1.00	0.45	0.97	0.22
Gastroc.	0.98	0.95	0.91	0.73	0.99	0.42

200 MHZ MEASUREMENTS (Old T Meter)

	T_1	T_2	Net Weight	$\%H_2O$	BF%/gm
			CONTROLS		
Soleus	13.6	15.7	0.1527	74.74	0.429
	13.2	16.3	0.1349	74.49	0.334
	13.6	16.2	0.1328	74.73	0.318
	12.3	22.3	0.1548	73.64	0.539
	12.7	21.3	0.1395	74.20	
	12.3	21.6	0.1746	72.60	0.158
$\bar{x}$	13.0	22.7	0.1482	74.07	0.356
SD	0.6	0.5	0.0158	0.83	0.141
			30 DAY SUSPENDED RATS		
Soleus	13.3	15.4	0.0793	72.71	0.045
	13.5	15.7	0.0842	71.97	0.028
	13.0	20.8	0.0652	69.40	0.082
	13.1	19.3	0.0650	71.73	
$\bar{x}$	13.2	20.0	0.0734	71.45	0.052
SD	0.2	1.1	0.0098	1.43	0.027

20 MHZ MEASUREMENTS (Old T Meter)

	T_1	T_2	Net Weight	$\%H_2O$	BF%/gm
			CONTROLS		
Gastroc.	12.8	16.0	2.0301	73.60	0.116
	13.0	16.3	2.5738	79.65	0.191
	13.3	15.4	1.9056	73.29	0.161
	12.6	22.1	2.0072	73.20	0.161
	12.8	20.4	1.9960	73.30	
	12.8	19.9	2.2651	74.08	0.147
$\bar{x}$	12.9	20.8	2.1363	74.52	0.155
SD	0.2	1.2	0.2470	2.53	0.027
			30 DAY SUSPENDED RATS		
Gastroc.	12.8	15.0	1.7423	73.49	0.049
	12.6	15.6	1.7081	73.59	0.066
	12.8	20.9	1.5406	73.67	0.062
	12.6	20.8	1.4318	73.76	
$\bar{x}$	12.7	20.8	1.6057	73.63	0.059
SD	0.1	0.1	0.1456	0.12	0.009
			SUSPENDED/CONTROL		
Soleus	1.02	0.95	0.49	0.96	0.15
Gastroc.	0.98	1.03	0.75	0.99	0.38

20 MHZ MEASUREMENTS (NEW)

	Rat	T_1	T_2
		CONTROLS	
Soleus	10F	315	29
	11F	329	26
Gastroc.	10F	308	26
	11F.	297	23

10 MHZ MEASUREMENTS (IBM)

	T_1	T_2
Soleus	-	-
Gastroc.	0.337	28.7
	CONTROL	
Soleus	0.330	35.8
Gastroc.	0.345	23.4

The above measurements of muscle in rats rear-limb suspended for 14 - 90 have shown that despite severe muscle atrophy and changes in muscle blood flow, T_1 and T_2 NMR parameters are within normal values. Possible explanations for this are that changes in blood flow, or sacrificing and removing the muscle specimen alters the NMR signal to mask the effect from atrophy. The alternative is that atrophy produced in this manner does not alter relaxation times unlike muscle dystrophy. A set of experiments were conducted to determine 1) whether NMR parameters are altered significantly with blood flow and 2) to determine if NMR signals are similar in muscles from live versus dead animals. Two rabbits, weighing 2.5 kg. were anesthetized and imaged with the 6 MHz whole body imager (head probe in). The pulse sequence was a 90° pulse followed by a train of 16, 180° pulses spaced at 3 msec. The rabbits were imaged with the cross-sectional slice just superior to the kidneys. Using a technique developed at Baylor (see attached), a calculated T_2 image was produced - 1) with the animal alive, 2) with the animal alive but with the descending aorta occluded, and 3) 15 minutes after sacrifice. using a region of interest cursor, the value of the supraspinal muscles was obtained for each image. The calculated T_2 was approximately 19 msec and was not altered by arterial occlusion or death.

HUMAN STUDIES

An initial series of images were taken of the lower limbs of one of the investigators using the spin echo technique and the 6 mHz instrument. Three slices were obtained corresponding to regions through the belly of the soleus, the belly of the gastrocnemius and the distal femur. These pictures demonstrated the potential to differentiate individual muscle groups and clearly image various structures. The possibility of monitoring differential muscle atrophy is apparent. As discussed previously we found that in the suspended rat model the soleus (slow twitch) atrophies 50% in two to four weeks while the gastrocnemius (fast twitch) atrophies 25%. Since the fluoride bedrest studies are in progress the opportunity to make measurements under controlled conditions where atrophy should occur is possible. In order to quantitate the NMR images in units of cm^2 or cm^3, the pixel size and slice thickness would have to be known each time an image is obtained. Since the pre and post bedrest images might be separated by weeks or months, a direct calibration is necessary. A jig was designed to rigidly hold the right limb immobile during NMR acquisition. A typical T_2 image requires about 4 minutes. A schematic of the device is given in Figure One. In addition to rigidly holding the leg, the jig unambiguously determines slice location, pixel size and thickness. This is accomplished by a series of machined grooves in the holder which are filled with an NMR sensitive material. After experimenting with a number of vegetable fat substances, Crisco was chosen to fill the grooves. Four grooves (A-D) are used for calibrating the pixel size and hence the x-y plane dimensions. The image length produced from the E grooves after simple geometric calculation gives slice thickness. The image of the series of grooves labeled F is used to calibrate the precise location on the jig where the NMR slice is acquired. This permits exact anatomical repositioning by carefully positioning the leg in the jig in the same manner each time. Calibration is accomplished by noting the distance between grooves A, E, and F. A digital histogram through the two spots of the F grooves gives a crude estimate of image resolution. The large tube labeled G is used to obtain calculated relaxation times which are used to monitor system stability for comparing tissue relaxation times.

All imaging to date has been accomplished using the 6 mHz Bruker magnet and head probe to enhance image resolution. Calf area images of two normal male volunteers were obtained. In one subject (swimmer) a series of 5 slices (A-E) 3 cm apart, starting from the heel were obtained. The sixth slice (F) was obtained at the level of the proximal tibia. The first volunteer subject was then removed from the magnet and a second volunteer subject (jogger) positioned within the magnet. Two slices were obtained 3 cm apart, starting at 35 cm from the heel. The second volunteer got back in and a slice (I) was obtained which corresponded to slice C to test reproducibility. The NMR technique was spin echo using a 180° slice select pulse followed 20 msecs later by a 90° read pulse and 16, 180° spin echo pulses separated by 9 msec. A delay of one second is used between the end of the spin echos and the next slice select pulse. Reconstruction was accomplished from 120 projections at 1.5° intervals in a collection matrix of 256 x 256. For each projection a series of 16 echoes were collected and reformatted into four echoes by summing successive echoes in groups of 4. After reconstruction, each of these are displayed as separate images. From these four images, T_2 and spin density images are computer calculated. The methodology and documentation for producing accurate calculated T_2 NMR images has been published by investigators at Baylor and a copy is included in the appendix.

Attached are copies of 4 images from slice C, figure 2, from the first volunteer. The upper left images of each are reconstructed from the first four echoes (CP1); the upper right image from the third set of four echoes (CP3); the lower left is the T_2 and the lower right the spin density image. Muscle contrast appears to be best in the images obtained during the latter portion of the echo train as evidenced by comparing CP3 vs CP1. There are four marker spots surrounding each image produced from NMR sensitive material in the jig. Since the distance between the points are known exactly, the pixel size can be calculated, which for this image sequence was 1.1 mm. The markings below the image are used to calculate slice thickness, 1.5 - 2.0 cm in this determination. Two spots which appear below and to the left of each image serve to unambiguously determine the distance from the subject's heel at which the NMR slice was taken. A pixel intensity vs distance histogram through these markers give an estimate of image resolution, <2 mm. Grossly, the two slices appear very similar, indicating adequate reproducibility for a scan through a given anatomical location. Bone width, cross-sectional areas and shape are readily obtained from CP1 or spin density images. Marrow, fat, vessels, and muscle are best distinguished in the T_2 calculated image.

NASA has considerable experience in image processing resulting from the remote sensing program (Earth Observations). Typically NMR imaging requires considerable image processing and therefore benefits from NASA technology. A number of techniques for combining multiple NMR images (spin density, T_1, T_2, early vs late spin echo) are being investigated such as a 3 color combination, parallelepiped, principal component, etc. In addition an effort is ongoing to improve NMR images, i.e., contrast, edge detection, resolution, signal to noise ratio. Figure 3 is a black and white image of CP1 slice C from subject number one using the shadow technique to enhance contrast. Figure 4 is a reconstructed image of this same slice using 3 color combination. The NMR picture was constructed by coding the CP1 picture red, CP3 green and the ratio of CP1/CP3 as blue. These three images are then combined to form the NMR picture of Figure 4. It is not clear at the present time what advantage these various display methods will have, but work is progressing to determine the optimum combination of resolution and contrast. For example, the highest S/N in the T_2 images is observed in CP1 while the greatest contrast is seen in CP3-4. Another series of images from T_1 experiments will result which will have different relative tissue intensities compared to T_2 images. Earth resource techniques allow the combination of several of the NMR images in various ways to produce enhanced information in a compact/accessible form. A more detailed description of these techniques is contained in Appendix B. One major objective is to be able to distinguish individual muscle groups. Figure 4 shows a considerable amount of anatomical detail. The soleus is clearly demonstrated as well as the lateral and medial lobes of gastrocnemius. Other muscles that appear to be observable are the anterior and posterior tibialis, peroneus longus and brevis, and the extensor hallucis and digitorum. The anterior and posterior tibial and preoneal vessels are clearly seen as are the compact bone and marrow of the tibia and fibula. It is expected that images such as Figure 4 will best demonstrate muscle size changes.

We are also attempting to characterize and quantitate tissue by differences in T_2. A preliminary classification is given below.

Tissue	T_2 (msec)	Color Code
Muscle	40 - 60	Red
Fascia	60 - 80	Magenta
Fat	85 - 126	Yellow
Marrow	122 - 138	Blue-White
Blood (vessels)	150 - 240	White Gray Scale
Bone	nil	Black

By assigning a color to pixels having these ranges of T_2 an image can be formed. Figure 5 is a T_2 colored image based on the above scheme. It is important to realize that the color scheme is not uniform but corresponds to the above ranges of T_2. Since we can internally calibrate the pixel size in cm^2 we can simply have the computer add up the number of pixels in a given T_2 range and hence determine the areas represented by that tissue. Limited repeat imaging was performed in both subjects 1 and 2. The results given below are for slices which are from approximately the same anatomical area in the two subjects. Subject 1 is a swimmer while subject 2 is a jogger/limited marathoner. The repeat images of subject 1 occurred on the same day as the original while those of subject 2 were separated by about 3 weeks.

Tissue Area from T_2 Reconstructed Images
Tissue Area (cm^2)

	Subject #1 (AL)					Subject #2 (HE)				
	Scan 1		Scan 2		area %	Scan 1		Scan 2		area %
	Area	T_2	Area	T_2		Area	T_2	Area	T_2	
	cm^2	msec	cm^2	msec		cm^2	msec	cm^2	msec	
Total Area	86.4		85.2		1.4	87.4		89.0		1.8
Muscle	43.5	39	41.4	38	4.8	59.3	38	59.1	39	0.4
Fat	18.6	109	21.4	107	14	14.4	98	14.6	98	1.4
Tibia Bone	4.20	*	3.27	*	24	5.05	*	5.17	*	2.3
Tibia Marrow	2.43	132	3.03	128	22	2.38	132	2.43	130	2.1
Circulation	2.2	172	1.1	167	58	.181	155	.181	155	0

(*) Low value; difficult to measure.

The total limb area was reproducible within about 1.5 % using T_2. Using cpl images however precision is about 0.2%. Despite a machine problem with the acquisition of scan 2 of Subject 1, precision of muscle fat, bone and marrow appear promising. As expected in the adult, the marrow of the extremity is mostly yellow/fatty marrow as reflected in the T_2 value which is close to subcu fat.

We have an approved human use protocol for performing NMR imaging in bedrest subjects. A copy of this protocol is contained in the appendix. To date 6 subjects have been imaged pre and post 5 weeks of bedrest. Each subject was repeated twice before and after bedrest. These results are now being analyzed at JSC. Table 1 and Table 2 summarize some of these early results.

We have shown that leg area measurements using NMR are possible with a precision of about 0.2%; fat and muscle cross-sectional area may be accurately measured in a given anatomical section; differential muscle atrophy can be quantitated. Table 1 gives the total and regional muscle area in mm^2 through the belly of the gastrocnemius pre and post 5 weeks of bedrest in 6 normal subjects. Each pre and post bedrest value represents the average of 2 slices separated by two cm with each slice measurement repeated. The mean and standard deviation is obtained from 4 area measurements. This region of the limb which includes both soleus and gastrocnemius varies less in area with limb position and therefore shows very good reproducibility, i.e., about 2 - 5%. Measurement of the soleus alone, which appears to demonstrate even larger percentage changes, are in progress. The mean loss of gastrocnemius and soleus cross-sectional area for all 6 subjects was 9% while the total muscle area loss was 6%.

The values in Table 2 are the average of 5 slices separated by 2 cm starting at a position through the belly of the soleus. Each series of slices is repeated therefore the mean and standard deviation are calculated from 10 NMR limb measurements. The reproducibility is within 4%. Data in Table 2 demonstrates a significant decrease in T_2 compatible with an increase in marrow fat. Slowly moving or stagnant blood has T_2 values considerably higher than fat. Table 2 also shows that no change in subcutaneous fat T_2 relaxation time occurred. It has been reported that the muscle water content of biopsied soleus muscles decreased following 8 hours of head down tilt bedrest. Tissue T_1 and T_2 values are very sensitive to tissue water. For example, a 2% change in tissue water may produce a 16% change in the relaxation time of tissue. Our studies with 5 weeks of horizontal bedrest indicate no change in tissue hydration since muscle T_2 relaxation times were not altered despite significant muscle atrophy; see Table 2.

TABLE I

Total and regional muscle area (mm^2) after 5 weeks of bedrest

-4cm section at level of gastrocnemius center

GASTROCNEMIUS + SOLEUS MEAN ± SD

Subject	Pre-Bedrest	Post-Bedrest	Δ %	P
36	6085 ± 446	5005 ± 328	-18	<0.001
37	*3970	4163 ± 57	5	0.04
39	4548 ± 138	3697 ± 108	-19	<0.001
42	4517 ± 79	4291 ± 80	-5	NS
46	3558 ± 137	3384 ± 168	-5	NS
47	4456 ± 73	3956 ± 12	-11	<0.001

* One measurement because of acquisition artifacts

TOTAL MUSCLE MEAN ± SD

36	8980 ± 472	8121 ± 384	-10	<0.001
37	6374	6519 ± 197	2	NS
39	6731 ± 281	6004 ± 211	-11	<0.001
42	7053 ± 70	6514 ± 140	-8	0.03
46	5326 ± 85	5307 ± 71	0	NS
47	6643 ± 9	6186 ± 6	-7	<0.001

TABLE 2

Preliminary Results of NMR limb imaging of bedrest subjects

(n=6) - Tissue T_2, pre vs post-bedrest

	MARROW, msec ± SD			MUSCLE, msec ± SD		FAT, msec ± SD	
	Pre	Post	Δ%	Pre	Post	Pre	Post
	135 ± 6	114 ± 7	-16	44 ± 1	52 ± 2	TBA*	
	147 ± 11	129 ± 17	-12	53 ± 2	53 ± 4	TBA*	
	130 ± 4	128 ± 4	-2	43 ± 2	46 ± 2	93†	93†
	132 ± 2	124 ± 3	-6	48 ± 2	47 ± 1	96†	104†
	149 ± 8	115 ± 2	-23	51 ± 3	48 ± 1	102†	100†
	145 ± 7	116 ± 2	-20	48 ± 1	50 ± 2	103†	94†
$\bar{x}$±SE	140 ± 3	121 ± 3		48 ± 2	49 ± 1	98 ± 2	98 ± 2
$\bar{\Delta}$%	-14			+2		0	
P	0.001			NS		NS	

*TBA - to be analyzed

† average of 2 measurements only

REFERENCES

1. Bloch F, Hansen WW, Packard M. Nuclear induction. Phys Rev 69:127, 1947.

2. Bloch F. Nuclear induction. Phys Rev 70:460-474, 1946.

3. Bloch F, Hansen WW, Packard ME. The nuclear induction experiment. Phys Rev 70:474-485, 1946.

4. Purcell EM, Torrey HC, Pound RV. Resonance absorption nuclear magnetic moments in a solid. Phys Rev 69:37-39, 1946.

5. Gadian DG, Radda GK. NMR studies of tissue metabolism. Ann Rev Biochem 50:69-83, 1981.

6. Ackerman JJH, Grove TH, Wong GG, Gadian DG, Radda GK. Mapping of metabolites in whole animals by 31P NMR using surface coils. Nature 282: 167-170, 1980.

7. Gordon RE, Hanley PE, Shaw D, Gadian DG, Radda GK, Styles P, Bore PJ, Chan L. Nature 287:736-737, 1980.

8. Grove TH, Ackerman JJH, Radda GK, Bore PJ. Analysis of rat heart in vivo by phosphorus nuclear magnetic resonance. Communicated by Britton Chance, October 26, 1979. Proc Nat Acad Sci USA; 77:299-302.

9. McLaughlin AC, Takeda H and Chance B. Rapid ATP assays in perfused mouse liver by 31 P NMR. Proc Natl Acad Sci 76(11):5445-5449, 1979.

10. Nunnally RL, Bottomley PA. Assessment of pharmacological treatment of myocardial infarction by phosphorus-31 NMR with surface coils. Science 211(4478): 77-88, 1981.

11. Ling CM, Foster MA, Hutchison JMS. Comparison of NMR water proton-T1 relaxation-times of rabbit-tissue at 24 MHz and 2.5 MHz (letter). Phys Med Biol 25:748-751, 1980.

12. Brooks RA. Nuclear magnetic relaxation in blood. IEEE Trans Biomed Eng BM-22:12, 1975.

13. Go KG, Edzes HT. Water in brain edema. Observations by the pulsed nuclear magnetic resonance technique. Archives Neurol 32:462, 1975.

14. Bakay L, Kurland RJ, Parrish RG, Lee JC, Peng RJ, Bartkowski HM. Nuclear magnetic resonance studies in normal and edematous brain tissue. Exp Brain Res 23:241, 1975.

15. Parrish RG, Kurland RJ, Janese WW, Bakay L. Proton relaxation rates of water in brain and brain tumors. Science 183:438, 1975.

16. Michael LH, Seitz P, McMilin-Wood J, Chang DC, Hazlewood CF, Entman ML. Mitochondrial water in myocardial ischemia: investigation with nuclear magnetic resonance. Science 208:1267-1269, 1980.

17. Damadian R, Minkoff L, Goldsmith M, Stanford M, Koutcher J. Tumor imaging in a live animal by field focusing NMR (FONAR). Physiol Chem Phys 8:61, 1976.

18. Hinshaw WS. Image-formation by nuclear magnetic-resonance sensitive-point method. J Appl Phys 47:3709-3721, 1976.

19. Mansfield P, Maudsley AA, Bainen T. Fast scan proton density imaging by NMR. J Phys (E) 9:271-278, 1976.

20. Lauterbur PC. Image formation by induced local interactions: examples employing nuclear magnetic-resonance. Nature 242:190-191, 1973.

21. Damadian R. U.S. Patent 3,789,832, filed March 17, 1972.

22. Bovee Wm, Getreuer KW, Smidt J, Lindeman J. Nuclear magnetic resonance and detection of human breast tumor. J Natl Cancer Inst 67:53-55, 1978.

23. Damadian R. Tumor detection by nuclear magnetic resonance. Science 171:1151-1153, 1971.

24. Doyle FH, Pennock JM, Orr JS, et al. Imaging of the brain by nuclear magnetic resonance. Lancet 2:53-57, 1981.

25. Hawkes RC, Holland GN, Moore WS, Worthington BS. Nuclear magnetic-resonance (NMR) tomography of the brain: a preliminary clinical-assessment with demonstration of pathology. J Comput Assist Tomogr 4:577-586, 1980.

26. Smith FW, Mallard JR, Reid A, Hutchison JMS. Nuclear magnetic resonance tomographic imaging in liver disease. Lancet i:963-966, 1981.

27. Young IR, Hall AS, Pallis CA, Legg NG, Bydder GM, Steiner RE. Nuclear magnetic resonance imaging of the brain in multiple sclerosis. Lancet ii: 1063-1066, 1981.

28. Whedon GD, Lutwak L, Rambaut PC, Whittle MW, Smith MC, Reid J, Leach CS, Stadler CR, Sanford DD. (1977) Mineral and nitrogen metabolic studies, experiment M071. In: Deitlein L (ed) Biomedical results from Skylab. U.S. Govt. Printing Office, Washington, D.C., pp 164-174.

29. Deitrick, JE, Whedon GD, Shorr E. Effects of immobilization upon various metabolic and physiologic functions of normal men. Am J Med 4:3-26, January 1948.

30. Birge SJ Jr, Whedon GD. Bone. In Hypodynamics and Hypogravics, p.213, M. McCally, Ed. Academic Press, New York, 1968.

31. Donaldson CL, Hulley SB, Vogel JM, Hattner RS, Bayers JH, McMillan D. Effect of prolonged bed rest on bone mineral. Metabolism 19(12):1071-1084, December 1970.

32. Thornton WE, Rummel JA. (1977) Muscular deconditioning and its prevention in space flight. In: Deitlein L. (Ed) Biomedical Results from Skylab. U.S. Govt. Printing Office, Washington DC, pp. 191-197.

33. Hazlewood CF, Chang DC, Nichols ML, Woesner DE. Nuclear magnetic resonance transverse relaxation times of water protons in skeletal muscle. Biophys J 14:583-606, 1974.

34. Singer JR, Crooks LE. Nuclear Magnetic Resonance Blood Flow Measurements in the Human Brain. Science 221:654-656, 1983.

35. Grant JP, Back C. NMR Rheotomography: Feasibility and Clinical Potential. Med Phys 9(2):188-193, 1982.

36. Moran PR. Evaluations of the Phase-Modulation Method for True Flow Imaging by NMR. Radiology 149(P):206, 1983.

37. Lent AH, Balkanyi LR, Compton RA, et al. Flow-Velocity Imaging by NMR. Radiology 149(P):237, 1983.

38. Mills CM, Brant-Zawadski M, Crooks LE, et al. Nuclear Magnetic Resonance: Principles of Blood Flow Imaging. Am J Neuro Roentgenol 4: 1161-1166, 1983.

39. Vinocur B. Tapping into blood flow with magnetic resonance. Diagnostic Imaging 48-52, 1984.

40. Booth, FW. Time course of muscular atrophy during immobilization of hind limbs in rats. J Appl Physiol: Respirat Environ Exercise Physiol 43(4) 656-661, 1977.

41. Booth, FW. Effect of limb immobilization on skeletal muscle. J Appl Physiol: Respirat Environ Exercise Physiol 52(5):1113-1118, 1982.

42. Fischbach, GD, Robbins N. Changes in contractile properties of disused soleus muscles. J Physiol Londod 201:305-320, 1969.

43. Hudlicka' O. Changes in blood flow and substrate utilization in skeletal muscle after tenotomy. Physiol Bohemoslov 22:497-504, 1962.

44. Hudlicka' O. Blood flow and oxygen consumption in muscles after section of ventral roots. Cir Res 20:570-577, 1967.

45. Morey-Holton E, Wronski TJ. Animal models for simulating weightlessness. Physiologist 24(6):suppl 45-48, 1981.

46. LeBlanc A, Marsh C, Evans H, Johnson P, Schneider V, Jhingran S. Bone and muscle atrophy with limb suspension in the rat. J Appl Physiology (in press), 1984.

47. Ilyina-Kakuyeva EI, Petrova NV, Portugalov VV. The effect of space flight on the skeletal musculature and nerve apparatus of the muscles (morphologic and cytochemical study). The Effect of Dynamic Factors of Space Flight on Animal Organisms. 100-106, 1979. (NASA Translation Document TM-75692).

48. Reis DJ, Wooten GF, Hollenberg M. Differences in nutrient blood flow of red and white skeletal muscle in the cat. Am J Physiol 213(3):592-596, 1967.

49. Meyer R, Kushmerick MJ, Brown TR. Application of 31P-NMR spectroscopy to the study of striated muscle metabolism. Am J Physiol 242:C1-C11, 1982.

50. Ross BD, Raddu GK, Gadian G, Esirl M, Smith JF. Examination of a case of suspected McArdles Syndrome by P-31 NMR. New England J of Med 304:1338-1339, 1981.

51. Dawson MJ. Quantitative analysis of metabolite levels in normal subjects by P-31 topical magnetic resonance. Bioscience Reports 2:727-733, 1982.

52. Gadian D, Ross B, Bore P, Raddu G, Hockady J, Taylor D, Styles P. Examination of a myopathy by P-31 NMR. Lancet, October 10, 774-779, 1981.

53. Tipton CM, Hargens AR, Gollnick PD, Mubarak SJ, Gonsalves MRs, Tucker BJ. Influence of head-down tilt on muscle to action and starting forces. American College of Sports Medicine (abstract), 1980.

54. Mansfield P, Morris PC. NMR imaging in biomedicine. p. 20 Academic Press, New York, 1982.

55. Thornton WE, Hoffler GW. (1973) Hemodynamic studies of the legs under weightlessness. In: Deitlein, L. (Ed). Biomedical Results from Skylab. U.S. Govt. Printing Office, Washington, D.C. pp. 324-329.

56. Thornton WE, Hoffler GW, Rummel JA. (1977) Anthropometric changes and fluid shifts. In: Deitlein, L. (Ed). Biomedical Results from Skylab. U.S. Govt. Printing Office, Washington, D.C. pp. 330-338.

57. Lockwood DR, Vogel JM, Schneider VS, Hulley SB. Effect of the diphosphonate EHDP on bone mineral metabolism during prolonged bed rest. J of Clinical Endo and Metab 41:533-541, 1975.

58. Schneider VS, McDonald J. Skeletal Calcium Homeostasis and countermeasures to prevent disuse osteoporosis. Calcif Tissue Int 36:S151-S154, 1984.

59. Dull TA, Henneman PH. Urinary hydroxyproline as an index of collagen turnover in bone. N Engl J Med 268:132, 1963.

60. Klein L, Lafferty FW, Pearson OH, Curtiss PH Jr. Correlation of urinary hydroxyproline, serum alkaline phosphatase and skeletal calcium turnover. Metabolism 13:272, 1964.

61. Prockop DJ,Kivirikko KI. Relationship of hydroxyproline excretion in urine to collagen metabolism-Biochemistry and clinical applications. Ann Intern Med 66:1243, 1967.

62. Harris WH, Heaney RP. Skeletal renewal and metabolic bone disease. N Engl J Med 280:193, 253, 303, 1969.

63. Minaire P, Meunier P, Edouald C, Bernard J, Courpron P, Bourrat J. Quantitative histological date on disuse osteoporosis; comparison with biological data. Calcif Tissue Res 17:57-73, 1974.

64. Morey-Holton E, Wronski TJ. Animal models for simulation of weightlessness. Physiologist 24(6):545-548, 1981.

65. Johnson PC. The erythropoietic effects of weightlessness. In Current Concepts in Erythropoiesis, edited C.R. Dunn, Chapter 12. John Wiley & Sons Ltd., 1983.

66. Tavassuli M. Marrow Adipose Cells and Hemopoiesis: an interpretative view. Exp Hematol 12:139-146, 1984.